Schweizerische Eidgenossenschaft
Confédération suisse
Confederazione Svizzera
Confederaziun svizra

Eidgenössisches Departement für
Umwelt, Verkehr, Energie und Kommunikation UVEK

Bundesamt für Energie BFE

Jahresbericht 11. November 2010

Layered Thermoelectric Converters (LTEC)

Auftraggeber:
Bundesamt für Energie BFE
Forschungsprogramm Elektrizitätstechnologien & -anwendungen
CH-3003 Bern
www.bfe.admin.ch

Auftragnehmer:
EMPA
Department of Solid State Chemistry and Catalysis
Überlandesstrasse 129
CH-8600 Dübendorf
www.empa.ch

Autoren:
Dimas Surya Alfaruq, EMPA, dimas.alfaruq@empa.ch
Anke Weidenkaff, EMPA, anke.weidenkaff@empa.ch

BFE-Bereichsleiter: Dr. Michael Moser
BFE-Programmleiter: Roland Brüniger
BFE-Vertrags- und Projektnummer: 153459 /102669

Abstract

$CaMn_{0.98}Nb_{0.02}O_{2.98}$ single crystals were obtained by zone melting under pressure to avoid manganese evaporation. The phase purity, composition and structure of the crystal was analysed with X-ray diffraction (XRD). The crystal growth was affected by the rod's quality, growth speed, atmosphere and pressure. Transmission electron microscopy (TEM) revealed structural intergrowth of $CaMnO_3$ and $CaMn_2O_4$ and of $CaMnO_3$ and $CaMnO_{3-x}$ that match quite well together in their lattices growth Finally, the Seebeck coefficient measured with a Physical Properties Measurement System (PPMS) was found to be higher than the calculated value. Our studies revealed the promising thermoelectric properties of $CaMn_{0.98}Nb_{0.02}O_{3\pm\delta}$ with ZT_{1000K}=0.32 and the contribution of twin domains to phonon scattering [3, 12]. The results contribute to a better understanding of the physical and chemical properties of manganese perovskite single crystals.

Objectives

Complex transition metal oxides, e.g. perovskites, have been shown to possess a number of interesting physical and chemical properties. What is more, perovskites have a very flexible crystal structure allowing to even improve their very attractive properties by cationic or anionic substitution or doping [1, 2]. Manganese perovskites, for instance, have been intensively studied in recent years as for their colossal magneto resistance (CMR) and high Seebeck coefficients [3-7]. These characteristics are the result of the mixed-valence state of manganese (Mn^{3+}/Mn^{4+}) in manganites [8]. Changing the Mn^{3+}/Mn^{4+} ratio by, for example, modification of the oxygen content will affect the materials properties [2].

Up to now, single crystal growth of $CaMnO_3$, especially when doped at the manganese site has not been extensively studied. Only a few research reports are available dealing with the crystallization of $CaMnO_3$ [9, 10] and Mo-doped $CaMnO_3$ [11]. However, doping at the manganese site has a particular influence on the thermoelectric properties of the compounds.

The goal was to prepare $CaMn_{0.98}Nb_{0.02}O_{3\pm\delta}$ single crystals by means of the floating zone (FZ) technique. The FZ technique is well suited for single crystal growth of compounds which melt congruently when the radiation of a halogen lamp is focused onto the sample rods. The aim of using this technique for the preparation of $CaMn_{0.98}Nb_{0.02}O_{3\pm\delta}$ single crystals was to reduce grain boundaries and their supposed effect on the physical and chemical properties of the material [9, 11, 13-16].

The growth process was studied and the single crystal was characterized. The Seebeck coefficient was measured in the temperature range of 5 - 400K

Experimental and Results

1. Experimental

Perovskite-type $CaMn_{0.98}Nb_{0.02}O_3$ samples were prepared by a soft-chemistry synthesis method. Stoichiometric quantities of Ca $(NO_3)_2 \cdot 4H_2O$ (Fluka, ≥99.0%) and $Mn(NO_3)_2 \cdot 4H_2O$ (Merck, 98%) were dissolved in distilled water. Citric acid (Alfa Aesar, +98%) was used as chelating agent and added in excess with a citric acid / metal cation (Mn and Nb) molar ratio of 2:1 in order to prevent precipitation. $NbCl_5$ (Aldrich, 99.0%) was added as alcoholic solution. The mixture was homogenized by stirring and then polymerized at 353 - 363 K for four hours with further continuous stirring. The polymeric complex compound was transferred to a ceramic bowl and maintained at 353 K overnight to evaporate the water. The obtained polymer xerogel was pre-decomposed by heating it at a rate of 20 K/h to a final temperature of 573 K. After crushing and grinding the voluminous product, the temperature was raised to 1073 K at a rate of 573 K/h and the sample was calcined for 6 h. The resultant single-phase powder was pre-densified at a force of 20 kN using a hydropress (Jean Wirtz, Germany) and then, after grinding, densely packed into latex tubes and hydrostatically pressed at 3948 atm using an oil pump (PSI, Villigen/Switzerland). High-density green body rods with 8-14 mm in diameter and 10-15 cm in length were obtained. The rods were vertically mounted in an aluminum oxide tube, heated to 1473 K at a heating rate of 573 K/h and sintered at this temperature for 15 h to with the objective of further densification.

Single crystals were grown in a four-mirror optical floating zone furnace (10000-H, *Crystal Systems Corp Japan*) with four 300 kW halogen lamps as heating source. The light beam reflections were focused on the tip of the rods. The homogeneity of the molten zone was maintained by clockwise and counterclockwise rotation of the feed rod and seed rod, respectively.

Previous attempts to grow single crystals had failed because the growth rate was too low (0.5 - 2 mm/h), the rod's rotation speed was too high (25 - 35 rpm) and the pressure and composition of the atmosphere (pure Ar or pure O_2) was not conducive. Therefore, crystal growth was performed at a pressure of 5 bar corresponding to a flow rate of Ar and O_2 of 0.4 L/min 0.1 L/min, respectively, aiming to decrease manganese oxide evaporation. The upper and lower shafts were rotated at 20 rpm. In order to obtain high-quality single crystal a growth rate of 4 mm/h was used. At this growth rate, however, small cracks appeared in the crystals because of phase transition of calcium manganese oxide.

The Laue X-Ray diffraction measurement was carried out at the Paul Scherrer Institut (PSI) in Villigen/Switzerland. The orientation of the unspecified crystal was determined by processing the data from a diffraction image representing the reciprocal crystal lattice using the "Orient Express" simulation program.

Phase purity and crystallinity of the powder was checked by XRD with a scan range of 5-80° 2θ using a Phillips X'Pert PRO MPD Θ-Θ System equipped with a linear X'Celerator detector. The diffraction data collected was processed with the X'pert High Score Plus software.

HRTEM analysis was performed with a Philips CM30 microscope. Scanning transmission in the dark field mode (STEM-HAADF) and EDX-EEL spectroscopy analysis were carried out using a Jeol-JEM 2200FS in-column filter and a Tecnai G2 F20 X-Twin postcolumn GIF filter. The high resolution STEM-HAADF image was obtained with a Jeol 2200FS in-column filter with 0.2 nm spot size. Cross-sections of the heterostructures were thinned using tripod polishing and a dimple grinder (Gatan Model 656). The final electron transparency was achieved with an ion-beam milling system (RES 101 from Baltec). The EELS energy resolution was 1 eV with probe currents in the range of 0.6 - 1 nA. Images were acquired and processed by means of the Digital Micrograph software.

The oxygen content was analysed by thermogravimetry (TGA), using a Netzsch STA 409 CD thermo balance under hydrogen-reduced atmosphere. Thermogravimetric reduction was performed by heating the sample to 1373 K at a heating rate of 10 K/min in a 20 vol.% H_2 / He atmosphere. Under these conditions, the single crystal is reduced according to eq.1 assuming that the final products are in their most stable oxidation states:

$$CaMn_{0.98}Nb_{0.02}O_{3-\delta}(s) + 0.97H_2(g) \rightarrow CaO(s) + 0.98MnO(s) + 0.01Nb_2O_5(s) + 0.97H_2O(g) \quad \text{eq. (1)}$$

The Seebeck coefficient of the single crystal was measured on a bar-shaped specimen (7, 5 x 1, 6 x 2, 82 mm^3) in the temperature range of 5 - 400 K using a physical properties measurement system (PPMS) from Quantum Design. The sample was placed in thermal transport option (TTO) fixture with an isothermal radiation shield to avoid heat radiation losses. The measurement was carried out in a cryostat under secondary vacuum (10^{-5} – 10^{-6} mbar).

2. Results and Discussions

2.1. XRP diffractograms of sintered rods

The soft chemistry synthesis method used for the polycrystalline rod production provides for the fast and homogeneous introduction of Nb into the Ca/Mn cation matrix [12, 17] due to the liquid reaction conditions. The use of highly compact rods is important for the success of the crystallization process. The high density prevents the liquid zone from entering into the feed rod by capillary action and inhibits bubble formation which can lead to zone instability during crystal growth. Compression at 4000 bar and sintering resulted in a rod density of ≥ 92%.

Phase purity of the samples was determined using XRPD. Figure 1 shows the diffractogram of sintered $CaMn_{0.98}Nb_{0.02}O_{3-\delta}$ rods.

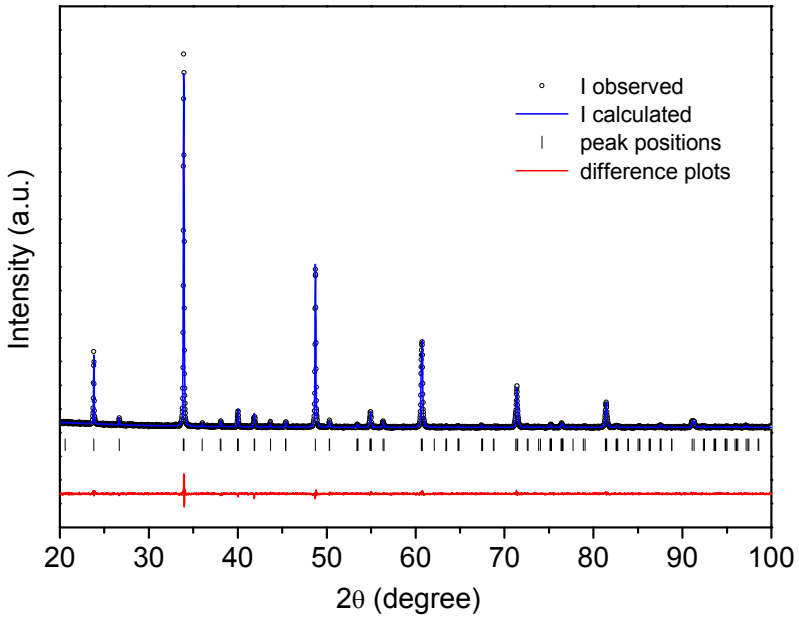

Figure 1: XRPD pattern and Rietveld refinement profile of $CaMn_{1-x}Nb_xO_{3-\delta}$ (x = 0.02). In addition, the difference between the observed and the calculated diffraction intensities (red line) along with the allowed Bragg positions (short vertical markers) are shown.

Name		$CaMn_{0.98}Nb_{0.02}O_{3-\delta}$
Radiation source		Lab x-ray $CuK_{\alpha 1}$
Wavelength (Å)		1.540598
Temperature (K)		298
2θ range (°)		20 - 100
Space Group		*Pbnm*
a (Å)		5.274941
b (Å)		5.288783
c (Å)		7.466673
V (Å^3)		208.3053
Ca	x	0.99599
	y	0.53258
	z	0.75000
	B_{iso} (Å^2)	0.84397
	occ.	0.5
Mn/Nb	x	0
	y	0
	z	0.5
	B_{iso}[a] (Å^2)	0.46541
	occ.	0.490/0.010
O1	x	0.07400
	y	0.98797
	z	0.75000
	B_{iso} (Å^2)	0.82029
	occ.	0.5
O2	x	0.71132
	y	0.78664
	z	0.53041
	B_{iso} (Å^2)	0.82027
	occ.	1.0
R_p		4.91
R_{wp}		6.37
χ^2		1.32

Table 1: Refined crystal structural parameters for $CaMn_{1-x}Nb_xO_{3-\delta}$ (X = 0.02).

Rietveld refinement of the XRD pattern of Nb-doped $CaMn_{1-x}Nb_xO_{3-\delta}$ (X = 0.02) was done using the FULLPROF software confirming the consistency with previously prepared material [12].

2.2 Laue diffraction pattern

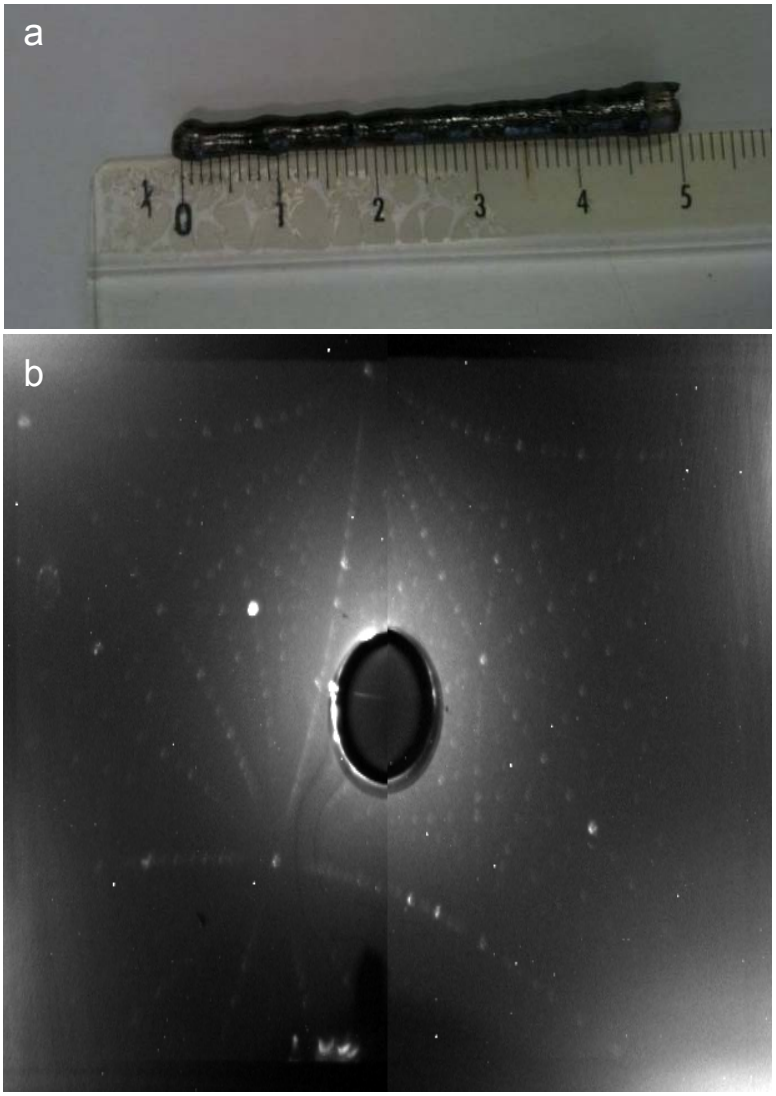

Figure 2: (a) Size of the boule (in cm), and (b) Laue pattern of the single crystal in (010) orientation (The picture was reshaped and the original aspect ratio was restored).

The growth rate is the most important parameter in order to obtain high-quality crystals using the FZ technique. Crystal size and the occurrence of cracks, second phases, bubbles and twinning depend on the growth rate [18]. In a previous study [11], excellent single crystal of the Ca-Mn-Mo-O system were produced at growth rates of 3 - 4 mm/h. Therefore, in our experiment a growth rate of 4 mm/h was applied. Lower growth rates resulted in secondary phase formation and increased manganese evaporation leading to coated tubes.

The experiment yielded a crystal of 5 cm in length (Fig. 2a). Starting from a polycrystalline seed rod, a single crystal started to formed within 1-2 cm of grown crystal. Fig 2b shows the Laue diffraction pattern of a polished top part of the crystal. The “Orient Express” simulation program suggests a (010) crystal orientation.

2.3. Nanostructure analysis by HRTEM

Nanostructure analysis of the crystal using HRTEM reveals the formation of $CaMn_2O_{4-\delta}$ and $CaMnO_{3-\delta}$ phases and their intergrowth with $CaMnO_3$. These minor phases arise from the melt during recrystallization as can be seen from the phase diagram of $CaMnO_3$ (Fig 3)

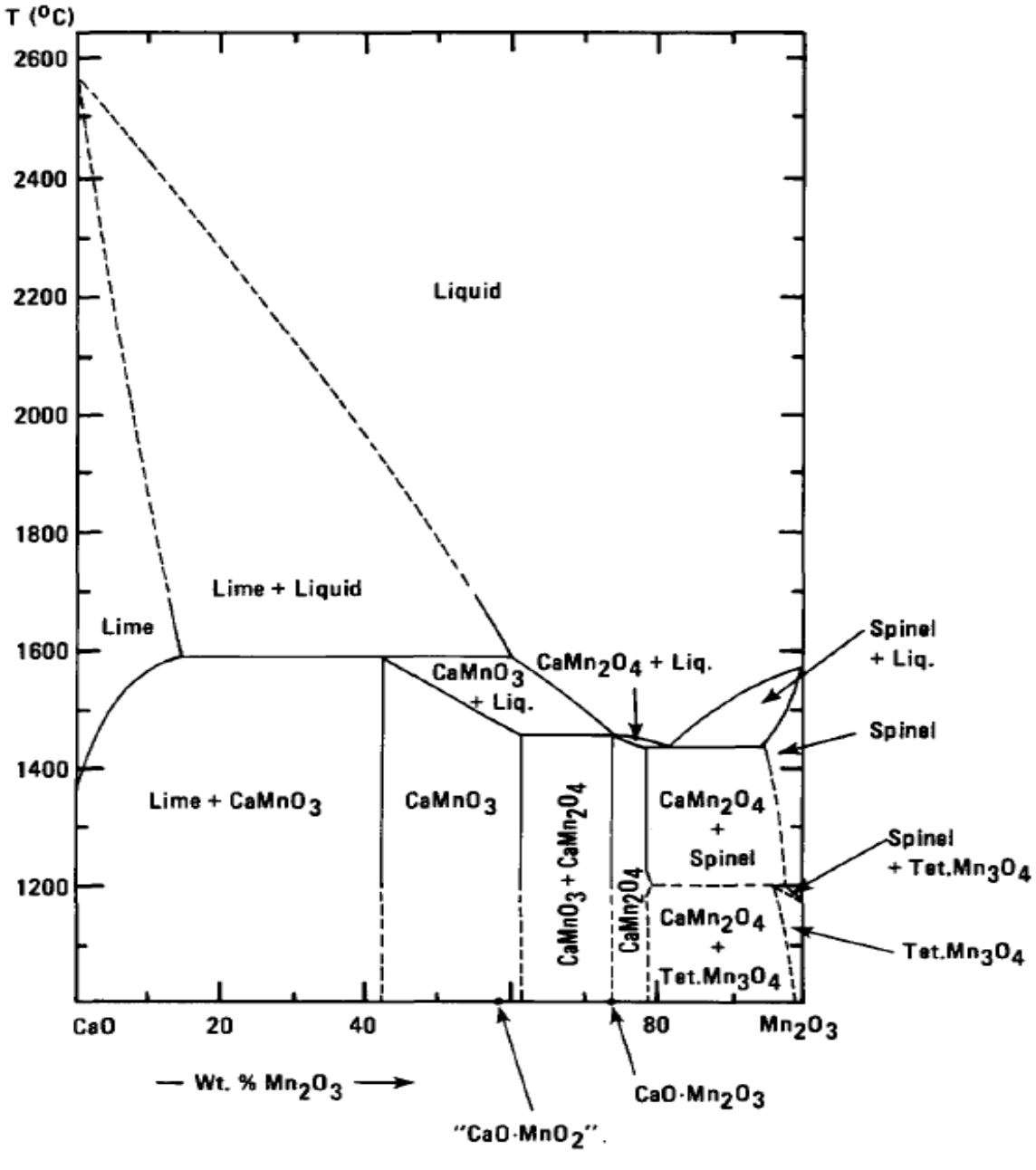

Figure 3: Phase diagram of $CaMnO_3$

The HRTEM image Fig. 4 shows the intergrowth of $CaMn_2O_{4-\delta}$ with two different zone axis orientations. The measurements are in good agreement with ref. code: 01-076-0516 (orthorhombic, Pmab (57), a=0.971 nm, b=1.003 nm, c=0.316nm).

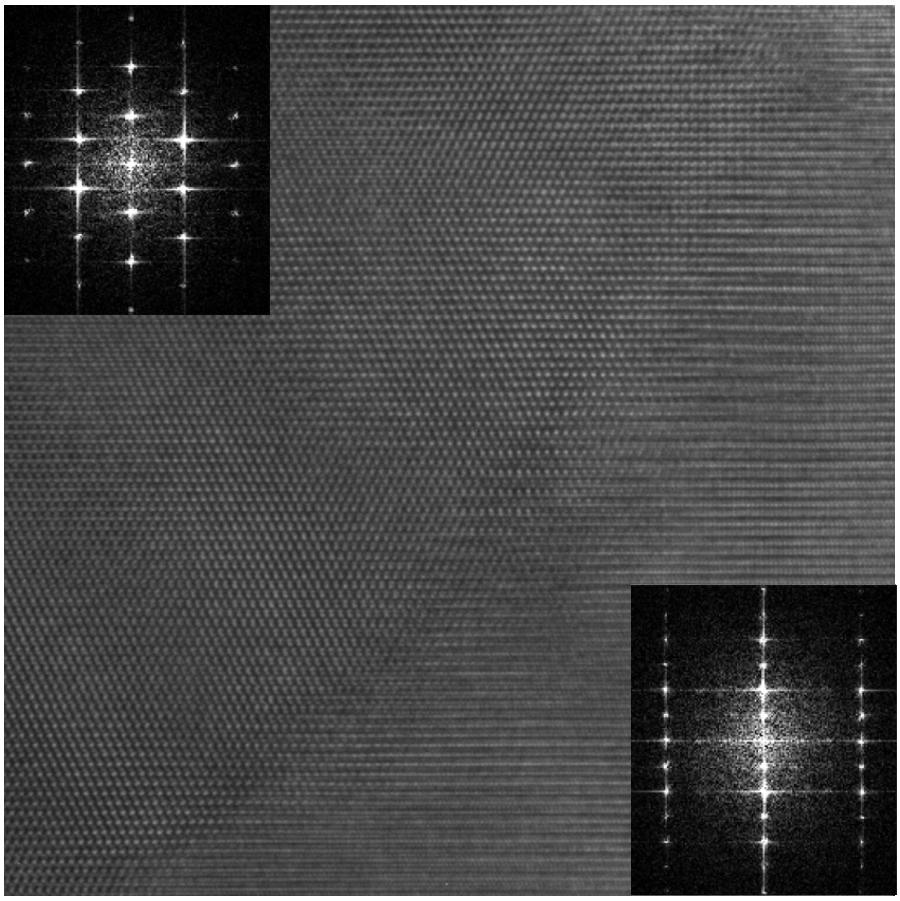

Figure 4: HRTEM image of the crystal showing intergrowth of $CaMn_2O_{4-x}$ with two different zone axis orientations.

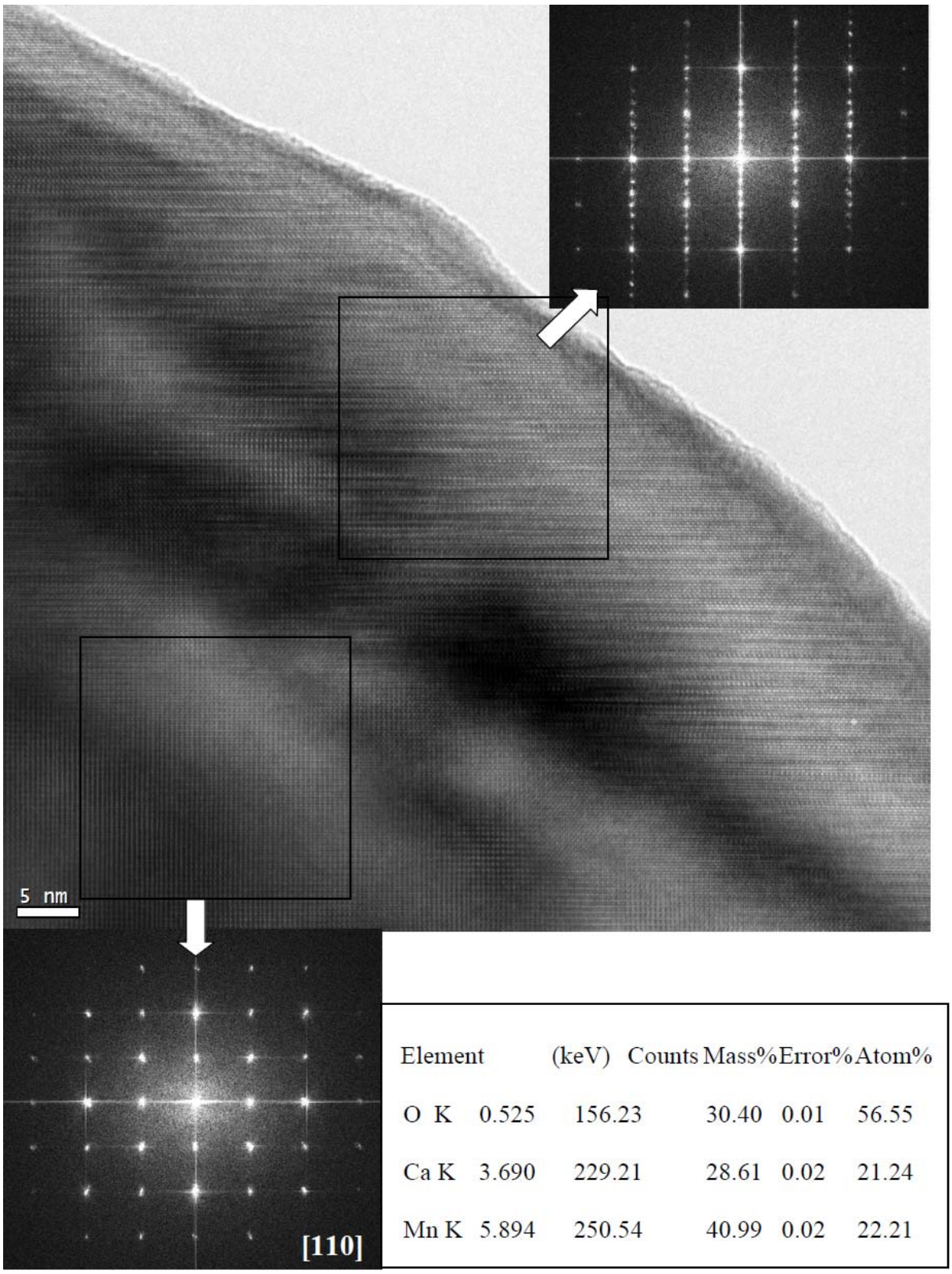

Element	(keV)	Counts	Mass%	Error%	Atom%
O K	0.525	156.23	30.40	0.01	56.55
Ca K	3.690	229.21	28.61	0.02	21.24
Mn K	5.894	250.54	40.99	0.02	22.21

Figure 5: Region with intergrowth of $CaMnO_3$ and $CaMn_{3-\delta}$

2.4. Oxygen content analysis

The thermogravimetric analysis resulted in a 10.56% mass reduction (*r*) of the crystal and is based on the following reaction equation:

$$CaMn_{0.98}Nb_{0.02}O_{3-\delta}(s) + 0.97H_2(g) \rightarrow CaO(s) + 0.98MnO(s) + 0.01Nb_2O_5(s) + 0.97H_2O(g) \quad \text{eq. (1)}$$

This mass reduction is defined as a ratio between the molecular masses (*M*) of the compounds before and after final reduction, which is described in the formula below.

$$r = \frac{(1 * M_{Ca} + 0.98 * M_{Mn} + 0.02 * M_{Nb} + (3-\delta) * M_O)}{(1 * M_{CaO} + 0.98 * M_{MnO} + 0.01 * M_{Nb2O5})} \quad \text{eq. (2)}$$

The calculation using the above formula shows an oxygen deficiency in the initial crystal compound with δ=0.02 confirming the amount of oxygen content is 2.98. When the oxygen content is already known, one can calculate the amount of Mn (III) and Mn (IV) in the compound. This suggests a chemical structure of compound of $CaMn^{III}_{0.04}Mn^{IV}_{0.94}Nb^{V}_{0.02}O_{2.98}$ and it is mixed together with $CaMn_{0.98}Nb_{0.02}O_3$ (based on TEM findings). Oxygen deficiency is accounted in the determination of the amount of Mn atoms in the compound [9, 10]. According to Jahn-Teller theory, adding Nb to Mn site will lead to formation of Mn^{3+} and Mn^{4+} [6] and the amount of Mn^{3+} depends on the amount of oxygen content of the crystal.

2.5. Seebeck coefficient

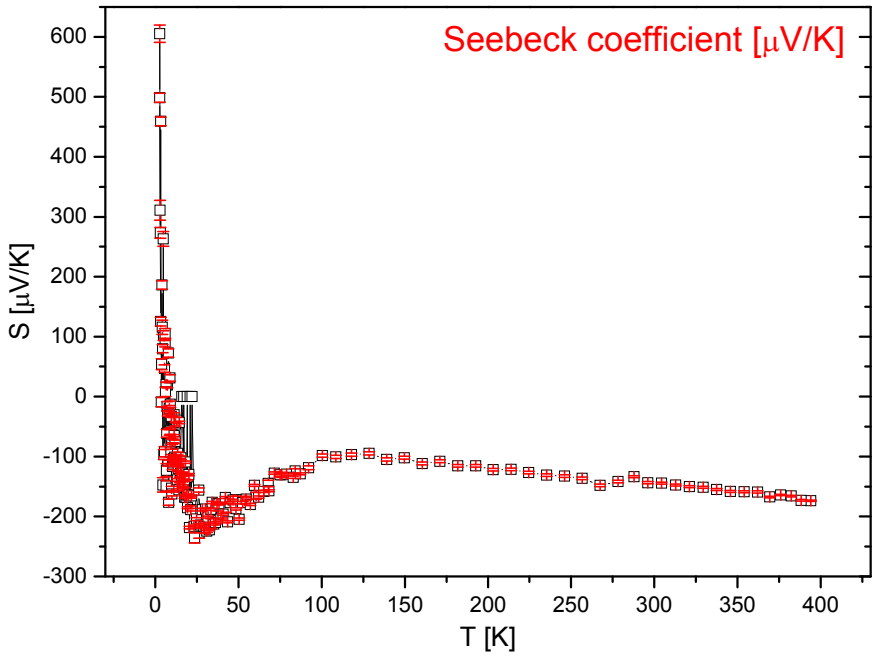

Figure 6: Seebeck coefficient of $CaMn_{0.98}Nb_{0.02}O_{2.98}$

Fig.6 shows the temperature dependence of the Seebeck coefficient of $CaMn_{0.98}Nb_{0.02}O_{2.98}$. The slope in the low temperature region is caused by the Colossal Magnetoresistance (CMR) which is common in calcium manganese compounds.

Based on the oxygen content calculated above the molar fraction of Mn^{3+} was determined to be 0.04. The theoretical evaluation of the Seebeck coefficient according to Kobayashi et al. [5] yielded a value of -195.26 μV/K at 400K. In contrast, the experimentally measured Seebeck coefficient was -173.52 μV/K at 400 K. The discrepancy in the results is caused by an

essentially higher Mn^{3+} content due to oxygen deficiency. Thus, electron hopping is enhanced by the double exchange mechanism in the Mn^{3+}-O-Mn^{4+} system leading to an increase of the electrical conductivity and consequently to a decrease of the Seebeck coefficient [19].

Conclusions 2010 and Outlook 2011

$CaMn_{0.98}Nb_{0.02}O_{3-\delta}$ single crystal were grown using a Floating Zone Furnace. HRTEM analysis revealed intergrowth of $CaMn_{0.98}Nb_{0.02}O_{3-\delta}$ and small quantities of $CaMn_2O_{4-\delta}$ and $CaMnO_{3-\delta}$.

Rietveld refinement did not indicate any secondary phases in the sintered rods. Therefore, the impurity phases can only be formed during the crystallization process in the Floating Zone Furnace.

Seebeck coefficient measured by PPMS has slightly higher value compared to published data [12] caused by higher amount of Mn^{3+} created from oxygen deficiency.

Additional investigation of the crystal structure by single crystal x-ray diffraction analysis will be required.

Future research will also focus on the production of thin films in order to improve the Figure of Merit (ZT) of the perovskite-type oxide materials.

References

[1] Töpfer, J. and J.B. Goodenough, Journal of Solid State Chemistry, 1997. **130**(1): p. 117-128.
[2] Rømark, L., et al., Journal of Materials Chemistry, 2002. **12**(4).
[3] Bocher, L., et al., Acta Materialia, 2009. **57**(19): p. 5667-5680.
[4] Briático, J., et al., Physical Review B, 1996. **53**(21): p. 14020.
[5] Kobayashi, W., et al., Journal of Applied Physics, 2004. **95**(11): p. 6825-6827.
[6] Maignan, A., et al., Physical Review B, 1998. **58**(5): p. 2758.
[7] Xu, G., et al., Solid State Ionics, 2004. **171**(1-2): p. 147-151.
[8] Reutler, P., et al., Journal of Crystal Growth, 2003. **249**(1-2): p. 222-229.
[9] Dubinin, S., et al., Physics of the Solid State, 2005. **47**(7): p. 1267-1272.
[10] Loshkareva, N.N., et al., Physical Review B, 2004. **70**(22): p. 224406.
[11] Miclau, M., D. Grebille, and C. Martin, Journal of Crystal Growth, 2005. **285**(4): p. 661-669.
[12] Bocher, L., et al., Inorganic Chemistry, 2008. **47**(18): p. 8077-8085.
[13] Balbashov, A.M., et al., Journal of Crystal Growth, 1996. **167**(1-2): p. 365-368.
[14] Kloc, C., S.W. Cheong, and P. Matl, Journal of Crystal Growth, 1998. **191**(1-2): p. 294-297.
[15] Mori, T., et al., Materials Letters, 2000. **42**(6): p. 387-389.
[16] Velázquez, M., et al., Journal of Crystal Growth, 2000. **220**(4): p. 480-487.
[17] Weidenkaff, A., Advanced Engineering Materials, 2004. **6**(9): p. 709-714.
[18] Koohpayeh, S.M., D. Fort, and J.S. Abell, Progress in Crystal Growth and Characterization of Materials. **54**(3-4): p. 121-137.
[19] Dresselhaus, M., et al., Physics of the Solid State, 1999. **41**(5): p. 679-682.